Journal of Materials Chemistry A

ROYAL SOCIETY OF CHEMISTRY

PAPER

View Article Online
View Journal | View Issue

Check for updates

Cite this: *J. Mater. Chem. A*, 2021, **9**, 3379

Alkylamino-terephthalate ligands stabilize 8-connected Zr^{4+} MOFs with highly efficient sorption for toxic Se species†

Anastasia D. Pournara,‡[a] Sofia Rapti,‡[a] Alexandros Valmas,[b] Irene Margiolaki,[b] Euaggelos Andreou,[c] Gerasimos S. Armatas,[c] Athanassios C. Tsipis,[a] John C. Plakatouras,[ad] Dimosthenis L. Giokas[ad] and Manolis J. Manos*[ad]

Received 30th November 2020
Accepted 11th January 2021

DOI: 10.1039/d0ta11653j

rsc.li/materials-a

Zirconium(IV) metal organic frameworks (MOFs) with low net connectivity and available intra-framework sorption sites constitute excellent sorbents for toxic anions. To expand this family of highly promising sorbents, it would be desired to develop new synthetic strategies aiming towards such materials. Here we show that the utilization of terephthalate ligands with small to medium size alkyl-amino functional groups comprises an effective approach towards microporous Zr^{4+} MOFs with 8-connected frameworks. The new MOFs were proved the most effective Se(IV) and Se(VI) sorbents ever reported, with exceptional sorption capacities (up to 272 $mg_{Se(IV)}$ g^{-1} and 290 $mg_{Se(VI)}$ g^{-1}), reusability, rapid sorption kinetics (≤3 min) and capability to sorb efficiently these anions in a very wide pH range (1–10), even in the presence of various competitive anions. The MOFs also display highly efficient sorption capability for the particularly toxic $SeCN^{-}$, with such property demonstrated for the first time for MOF materials.

Introduction

In the last two decades, metal–organic frameworks (MOFs), based on metal ions or clusters connected *via* extended polytopic ligands, have attracted considerable attention due to their structural diversity, high porosity and potential applications in various fields.[1–6] MOFs with ion-sorption properties seem very promising for use in wastewater treatment.[7–12] Such MOFs exhibit a highly ordered porous structure (in contrast to amorphous organic resins) in combination with a large variety of organic binding groups (not present in purely inorganic materials) and thus, they may be considered as a next generation of ion-sorbents. Among metal organic ion sorbents, Zr^{4+} MOFs are probably the most promising ones combining a number of important features, such as robustness (stability from extremely acidic to alkaline conditions), high porosity, capability to incorporate various functional groups and ease of synthesis.[13,14] In a recent work, we described $H_{16}[Zr_6O_{16}(H_2PATP)_4]Cl_8 \cdot xH_2O$ (**MOR-2**) (H_2PATP = 2-((pyridin-1-ium-2-ylmethyl)ammonio) terephthalate), a new microporous Zr^{4+} MOF featuring an 8-connected net.[15] The isolation of **MOR-2** with a lower net connectivity than the usual (12-connected) for Zr^{4+} MOFs with terephthalate ligands was attributed to the presence of the bulky substituent in the H_2PATP ligand, which likely prevents incorporation of more than 8 ligands per Zr_6 cluster due to steric interactions. **MOR-2** showed an extraordinary sorption capacity for Cr(VI), which is attributed not only to the favourable ion exchange of guest Cl^{-} anions by Cr(VI) species and Cr(VI)-functional group interactions but also to the ligation of Cr(VI) anions into the Zr_6 cluster replacing the labile terminal ligands of the pristine material. Thus, the decreased net connectivity of **MOR-2** led to enhanced porosity (compared to an hypothetical Zr^{4+}–H_2PATP 12-connected MOF which would be non-porous) and in a substantial improvement of the Cr(VI) sorption properties related to those of usual 12-connected Zr^{4+} MOFs. Furthermore, **MOR-2** has shown remarkably high sorption capacities for ReO_4^{-}/TcO_4^{-}, which were due to the capability of the MOF to bind Re(VII)/Tc(VII) into the Zr_6 clusters.[16] These results reported from our group and also the pioneering work on the anion sorption properties of NU-1000 (ref. 17–19) (which also exhibit an 8-connected framework) indicate Zr^{4+} MOFs with decreased net-connectivity as a source of highly promising sorbent materials for anionic pollutants. Thus, it appears very

[a]*Department of Chemistry, University of Ioannina, GR-45110 Ioannina, Greece. E-mail: emanos@uoi.gr*

[b]*Department of Biology, Section of Genetics, Cell Biology and Development, University of Patras, GR-26500 Patras, Greece*

[c]*Department of Materials Science and Technology, University of Crete, GR-71003 Heraklion, Greece*

[d]*Institute of Materials Science and Computing, University Research Center of Ioannina, Ioannina, GR-45110, Greece*

† Electronic supplementary information (ESI) available: Experimental procedures; thermal analyses data; X-ray powder diffraction studies and other characterization data for the reported MOFs; ion sorption data; characterization of ion-loaded materials; theoretical calculations. CCDC 2017777–2017786. For ESI and crystallographic data in CIF or other electronic format see DOI: 10.1039/d0ta11653j

‡ These two authors contributed equally.

attractive to develop synthetic strategies towards new Zr^{4+} MOFs with low-net connectivity in order to discover new materials with enhanced properties and potential for practical applications in environmental remediation.

Herein, we report four new microporous Zr^{4+} MOFs with the general formula $H_{16}[Zr_6O_{16}(RNH\text{-}BDC)_4]\cdot$solvent (RNH-$BDC^{2-}$ = 2-alkyl-amine-terephthalate; R = ethyl-, **ET-MOF**; R = propyl-, **PROP-MOF**; R = isobutyl-, **SBUT-MOF**; R = *n*-butyl, **BUT-MOF**). The new MOFs exhibit an 8-connected framework and display enhanced porosity (BET surface areas up to 832 $m^2\ g^{-1}$) compared to **MOR-2** (BET surface area = 354 $m^2\ g^{-1}$), the only previously reported Zr^{4+}-terephthalate MOF with 8-connected net. These materials have shown excellent Se(IV/VI) sorption properties, with fast/selective capture of these anionic species under a variety of conditions. The Se(IV)/(VI) maximum sorption capacities of alkylamino-functionalized MOFs are the highest reported for MOF materials and most of other sorbents. Moreover, these MOFs were proved highly efficient for sorption of $SeCN^-$ species, which is one of the most dangerous pollutants found in oil refinery and mining wastewater.[20] In fact, this is the first time that MOF materials have been tested for $SeCN^-$ capture. Overall, the present work demonstrates the use of terephthalic ligands with relatively small-sized functional groups as an effective method towards the isolation of porous Zr^{4+} MOFs with low net-connectivity and highly promising anion sorption properties.

Results and discussion

(a) Synthesis and structural characterization

As we mentioned in the introduction, the stabilization of an 8-connected framework in **MOR-2** was explained on the basis of the steric interactions between the bulky 2-picolylamino functional groups of the MOF that do not favour the formation of the usual 12-connected framework of Zr^{4+}-terephthalate materials.[15] As a next step in this research, it would be interesting to check if the presence of relatively small-sized functional groups (instead of bulky ones) in the terephthalate ligands will also lead to the stabilization of a framework with net connectivity <12. In that case, the resulting materials would combine low net connectivity-intra-framework anion sorption sites and enhanced surface areas compared to that of our previously reported **MOR-2** material. In this context, we decided to synthesize Zr^{4+} MOFs with alkyl (ethyl, propyl, isobutyl, *n*-butyl)-amino-BDC^{2-}, *i.e.* ligands with functional groups which are only slightly to moderately elongated compared to the functional groups (*i.e.* $-NH_2$) of the well-known UiO-66-NH_2 displaying 12-connected framework. A variety of synthetic approaches have been applied in order to isolate crystalline Zr^{4+} MOFs with the alkyl-amine-BDC^{2-} ligands and finally, highly crystalline Zr^{4+} MOFs with ethyl, propyl, isobutyl or *n*-butyl-amino-terephthalate ligands were isolated in good yield and purity. The results from thermal analyses indicated that these Zr^{4+} MOFs contain 4 terephthalate ligands per formula unit, which is consistent with 8-connected framework structures (Fig. S1–S4, Tables S1 and S2†). Unfortunately, these MOFs could not be isolated as single crystals and thus, powder X-ray diffraction (PXRD) methods were applied to determine and refine their structures. The PXRD patterns of the MOFs were indexed successfully in the tetragonal crystal system and

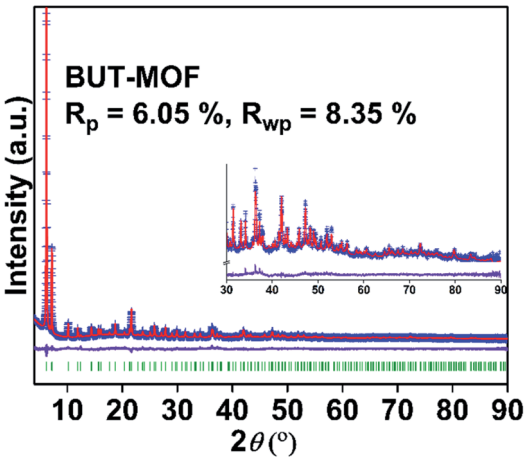

Fig. 1 Rietveld plot of **BUT-MOF**. Blue crosses: experimental points; red line: calculated pattern; violet line: difference pattern (exp. – calc.); green bars: Bragg positions. Inset: magnification of the 2θ region 30–90°.

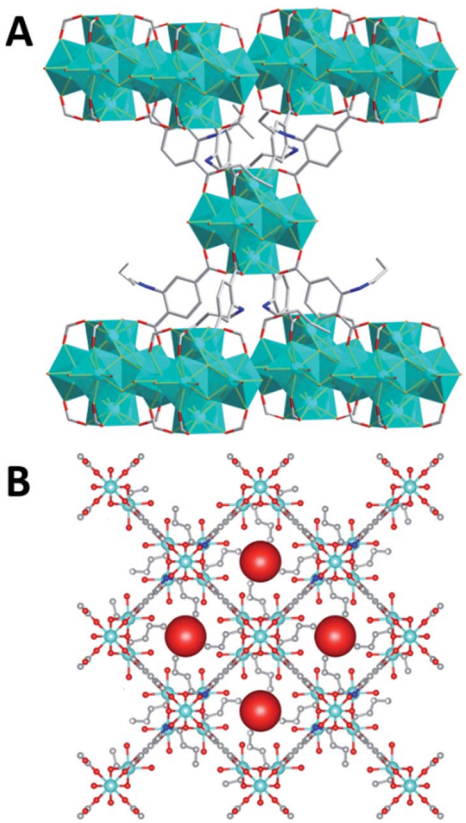

Fig. 2 (A) Representation of the cluster connectivity in **BUT-MOF**. (B) The framework structure of **BUT-MOF** viewed down the *c*-axis. For clarity, to eliminate the positional disorder of butyl-groups, the structure of the MOF is shown as the low symmetry *I*4̄ model. H atoms were omitted. Color code: Zr, cyan; N, blue; O, red; C, grey. The large red spheres denote the pores in the structure of **BUT-MOF**.

structureless refinement was performed choosing the space group $I4/m$. Then, we built 8-connected models of the MOFs' structures, which were further optimized *via* simulated annealing methods. These models were used as starting points for Rietveld refinements. The results of these refinements confirmed the accuracy of the selected structural models (Fig. 1, S5–S8 and Table S3†).

In the structures of the MOFs (Fig. 2 and S9–S12†), each Zr_6 cluster contains eight terminal (OH^-/H_2O) ligands on the equatorial plane, besides the bridging O^{2-}/OH^- and alkylamino-BDC^{2-} groups. The connectivity of the clusters is consistent with a **bcu** network (Fig. 2 and S9–S11†). The 2-alkylamino substituents of the ligands are directed to the center of the network pores and solvent molecules (DMF and H_2O) fill the space left available in the structures of the MOFs (Fig. S12†).

(b) Other characterizations

Field emission-scanning electron microscopy (FE-SEM) revealed that the new MOFs are composed of nanoparticles with a polyhedral shape and average size of ~66 nm (Fig. 3 and S13†). FT-IR spectra (Fig. S14†) showed characteristic absorptions of the alkyl-amino ligands (*e.g.* intense peaks at ~2900 cm^{-1} due to alkyl-chain of the ligands). ^1H NMR data (ESI†) obtained after digesting the MOFs in highly alkaline D_2O solution confirm the molecular integrity of the linkers in the MOFs, *i.e.* no loss of alkyl chains of the ligands was identified. Nitrogen physisorption measurements carried out at 77 K for the activated **MOF** samples showed typical type-I adsorption–desorption isotherms, characteristic of microporous solids (Fig. 4). The Brunauer–Emmett–Teller (BET) surface area of **ET-MOF**, **PROP-MOF**, **SBUT-MOF** and **BUT-MOF** were found equal to 832, 580, 556 and 609 $m^2\ g^{-1}$ respectively. The BET surface areas are in very good agreement with those predicted based on the crystal structure of the MOFs, thus providing a strong evidence for the accuracy of the determined structural models. Specifically, the theoretical surface areas calculated using the poreblazer program[21,22] were found 908, 573, 563 and 547 $m^2\ g^{-1}$ for **ET-MOF**, **PROP-MOF**, **SBUT-MOF** and **BUT-MOF** respectively. CO_2 adsorption isotherms recorded up to 1 bar at 273 K indicated sorption capacities of 2.78, 1.08, 1.26 and 1.34 mmol g^{-1} for the **ET-MOF**, **PROP-MOF**, **SBUT-MOF** and **BUT-MOF** materials respectively (Fig. S15†). Analysis of CO_2 adsorption data with the

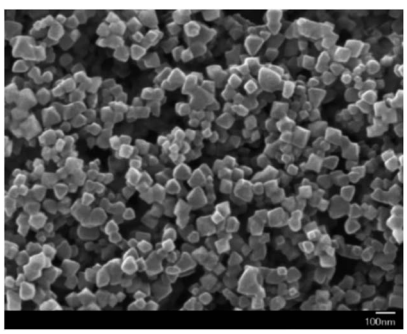

Fig. 3 FE-SEM image of BUT-MOF nanoparticles.

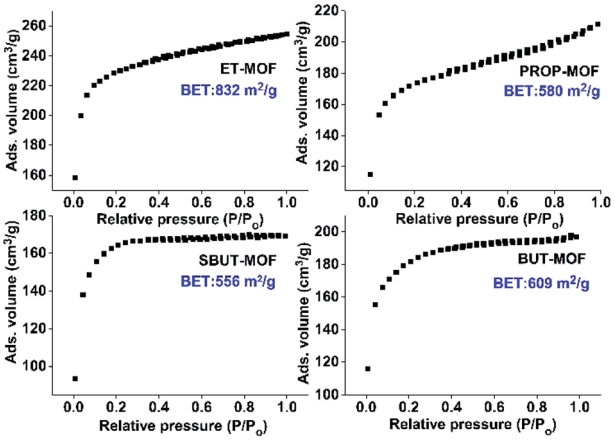

Fig. 4 N_2 sorption isotherms (77 K) for ET-MOF, PROP-MOF, SBUT-MOF and BUT-MOF.

density functional theory (DFT) suggests that **ET-MOF**, **PROP-MOF**, **SBUT-MOF** and **BUT-MOF** display microporous structure with pore sizes of 5.5–8.5 Å (Fig. S16†). The pores sizes for **ET-MOF**, **PROP-MOF**, **SBUT-MOF** and **BUT-MOF** found from poreblazer were 4–7 Å, which are relatively close to those determined from the gas sorption data. We should also note that the MOFs show excellent stability from extremely acidic (4 M HCl) to alkaline conditions (pH ~ 11) (Fig. S17 and S18†). In fact, the acid and base-treated materials are highly crystalline, so we were able to provide Rietveld refinement data (Fig. S17 and Table S3†).

(c) Anion sorption properties

The new MOFs with labile terminal ligands in the Zr_6 clusters and relatively high surface areas seem ideal sorbents for capture of anions. In the present work, we targeted on the sorption of Se anionic species, specifically selenite or Se(IV) (being in the form of $HSeO_3^-$ and SeO_3^{2-} at neutral and alkaline solutions (pH > 9) respectively), selenate or Se(VI) (being in the form of SeO_4^{2-} for pH > 2) and $SeCN^-$ anions.[23,24] Se species are considered particularly toxic and as a result, World Health Organization (WHO) and the European Union (EE) recommended a maximum selenium concentration in drinking water of only 10 ppb (the corresponding value suggested by US-EPA is 50 ppb). Though the attention has been mainly paid on the selenite and selenate, the selenocyanate anions ($SeCN^-$) are also present in wastewaters from oil refining and mining industries.[20]

The activation of the MOFs was performed by treatment with HCl, in order to protonate the amine groups and induce cationic charge to the frameworks.[15,16] Although sorption investigations have been conducted for all reported MOFs, detailed studies were performed only for **BUT-MOF**.

(i) Kinetic studies. Sorption studies for the activated **BUT-MOF** revealed remarkable fast capture of Se(IV) and Se(VI) oxoanions (Fig. 5). Specifically, the equilibrium time was 3 and 1 min for Se(IV) and Se(VI) sorption respectively. Remarkably, ≥99.8%% removal was achieved for Se(IV) and Se(VI) oxoanions after only 1–2 min of solution-MOF contact. The final

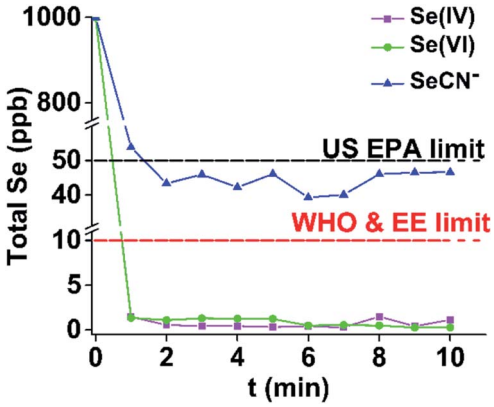

Fig. 5 Sorption of Se(IV), Se(VI) and $SeCN^-$ by **BUT-MOF** *vs.* time (initial total Se concentration was 1000 ppb, pH ~ 7).

concentrations of total Se were ≤1 ppb, which is well below the acceptable limit for Se (10 ppb) in water. The kinetics for the sorption of Se(IV) anions was fitted with first order model (Fig. S19 and Table S4†), whereas no fitting for Se(VI) sorption kinetics was possible due to the extremely fast capture of Se(VI) species by **BUT-MOF**.

Motivated by the fact that no $SeCN^-$ sorption data were reported for MOFs, we have also studied the sorption of $SeCN^-$ by **BUT-MOF**. The kinetics study revealed that the sorption of $SeCN^-$ by **BUT-MOF** was very fast with an equilibrium time of 2 min and removal capacity ≥95.6%. Due to the particularly rapid capture of $SeCN^-$ by **BUT-MOF**, fitting of the $SeCN^-$ sorption kinetics was not feasible.

(ii) Sorption isotherm studies. As a second step of our studies, we have determined the sorption isotherms (Fig. 6). The results found from the Se(VI) and $SeCN^-$ sorption isotherms were rather unusual. Thus, the Se(VI) sorption isotherm consists of two components, one for the low concentration range (1.8–635 ppm) and a second for the high concentration region (635–1800 ppm). Such a two-phase profile can be due to a combination of surface binding and pore filling processes, as shown recently for the As(III) sorption of a Zr^{4+} MOF.[25] At lower concentrations, Se(VI) anions are trapped mainly in the surface of particles *via* electrostatic interactions, whereas at high concentrations Se(VI) species diffuse into the pores and interact strongly with the MOF's framework. The data at low concentrations can be described with the Langmuir model, whereas the data at high concentration range follow the Langmuir–Freundlich model (Table S5†). The total Se(VI) sorption capacity is 226 $mg_{SeO_4^{2-}}$ g^{-1}, of which 115 $mg_{Se(VI)}$ g^{-1} are captured at the surface of the particles and 111 $mg_{Se(VI)}$ g^{-1} are trapped into the framework. The latter quantity of Se(VI) corresponds to 1.9 equivalents per formula unit of the MOF. Similarly, $SeCN^-$ sorption isotherm is also composed of two components, which are also attributed to surface and intra-framework complexation of the $SeCN^-$ anions. The total $SeCN^-$ sorption capacity was found 316 mg_{SeCN^-} g^{-1}, with 147 and 169 mg captured at the surface and framework respectively. The framework sorption capacity corresponds to 3.7 equivalents per formula of the MOF. The $SeCN^-$ sorption data at low and high concentration levels fit to the Langmuir and Langmuir–Freundlich models respectively (Table S6†). We should also note that the other MOF analogues (**ET**, **PROP**, **SBUT-MOFs**) have also shown Se(VI) and $SeCN^-$ sorption isotherms with two components (Fig. S20, S21, Tables S5 and S6†) and maximum sorption capacities of 240–290 and 312–361 mg g^{-1}, respectively. In contrast, the Se(IV) sorption isotherms of **BUT-MOF** and other analogues do not exhibit obvious two-step profile (for an explanation see below) and can be fitted with the Langmuir model showing maximum sorption capacities up to 272 $mg_{HSe_O^{3-}}$ g^{-1} (Fig. 6, S22 and Table S7†). The mechanism of sorption of the various anions by **BUT-MOF** is discussed below in more detail.

(iii) pH-dependent sorption studies. Sorption experiments were also carried out by varying the pH of the solutions. According to the results of Fig. S23, **BUT-MOF** can capture the toxic anions in very a wide pH range, from highly acidic to alkaline aqueous solutions. Specifically, the removal of Se(IV), Se(VI) and $SeCN^-$ was ≥99.6, ≥97 and ≥90% respectively in the pH range 1–10. The high capability of **BUT-MOF** to absorb Se species even under strong acidic conditions (pH ~ 1) points to potential applications related to the remediation of Se-containing petroleum refinery effluents which are strongly acidic (pH ≤ 1).[26] Furthermore, isotherm sorption studies conducted for Se(IV) at pH ~ 9.5 revealed relatively high sorption capacity (118 ± 3 $mg_{SeO3^{2-}}$ g^{-1}) (Fig. S24†).

(iv) Selectivity studies. We have also investigated the sorption of Se(IV), Se(VI) and $SeCN^-$ in the presence of common

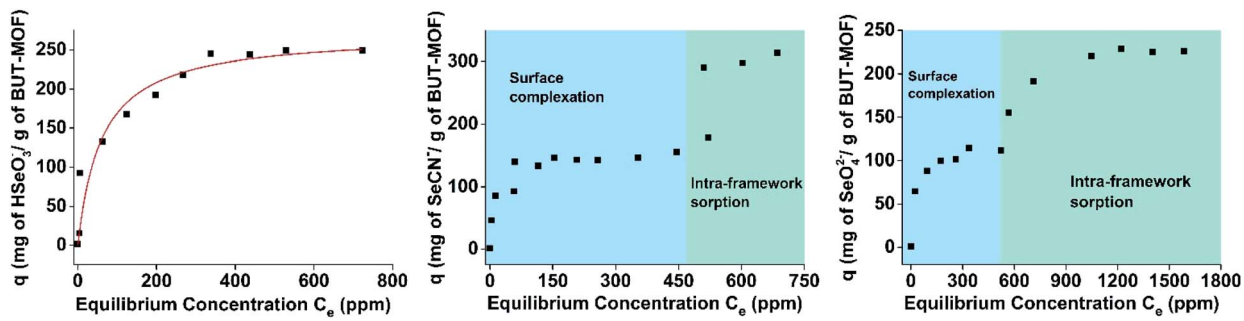

Fig. 6 Se(IV), $SeCN^-$ and Se(VI) sorption isotherms for **BUT-MOF** at pH ~ 7. The solid line in the Se(IV) sorption isotherm represents the fitting of the data with the Langmuir model.

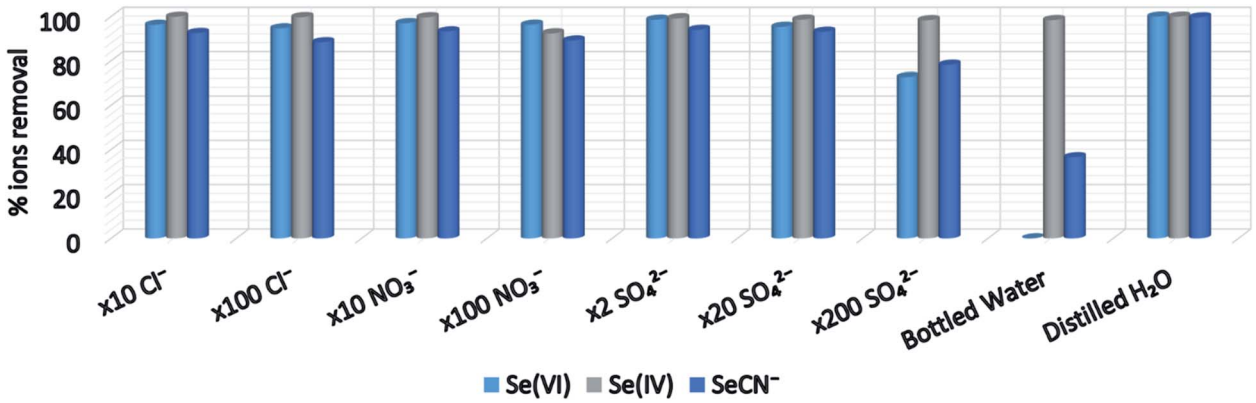

Fig. 7 Se(IV), Se(VI) and $SeCN^-$ sorption data for **BUT-MOF** in the presence of various competitive anions. Bottled water contained Ca^{2+} 93.1 ppm, Mg^{2+} 1.9 ppm, K^+ 0.7 ppm, Na^+ 2.6 ppm, HCO_3^{2-} 299 ppm, Cl^- 8.7 ppm, SO_4^{2-} 12 ppm, NO_3^- 7.9 ppm, pH = 7 ± 0.02. The initial total Se concentration was 1 ppm in all sorption experiments.

competitive anions such as Cl^-, NO_3^- and SO_4^{2-}. The data obtained indicated that selenite sorption is not affected by any of competitive anionic species and high removal capacities (>98%) were obtained even in the presence of 200-fold excess of SO_4^{2-} anions (Fig. 7). Similarly, selenate and selenocyanate sorption is not influenced by high concentrations of most competitive anions. At 200-fold excess of SO_4^{2-}, however, selenate and selenocyanate sorption decreases to ~73 and 78% respectively (Fig. 7). The efficient removal of Se species by the **BUT-MOF** in the presence of high sulfate concentrations is particularly important for applications in environmental remediation, as SO_4^{2-} is the major ion species during Se removal from wastewater.[20,26,27]

(v) Application in real water samples. In order to investigate whether **BUT-MOF** is suitable for Se sorption in genuine water samples, we performed tests with bottled water solutions intentionally contaminated with traces of Se species (initial total Se concentration = 1 ppm). Such samples contained several competitive anions including Cl^-, NO_3^-, SO_4^{2-} and HCO_3^- (as well as several cations, see Fig. 7 caption). Specifically, the molar concentration of Cl^-, NO_3^-, SO_4^{2-} and HCO_3^- were 16, 11, 16 and 230 higher than that of Se anionic species. Despite the presence of such high excess of these competitive anionic species, the selenite removal was found similar (>98%) to that determined in the absence of competitive anions (Fig. 7). Surprisingly, no SeO_4^{2-} sorption was observed and the $SeCN^-$ capture was ~36.5% (Fig. 7). Similar results have been also obtained for the other MOF analogues (Table S8†). An explanation for the enhanced affinity of **BUT-MOF** and other analogues towards Se(IV) is provided below.

(vi) Regeneration–reusability studies. The material can be regenerated by treating the ion-loaded MOF samples with 4 M HCl solution. The regenerated samples were re-loaded with the Se(IV), Se(VI) or $SeCN^-$ anions showing the same sorption capacity as that of pristine MOF. The regeneration and reusability of the **BUT-MOF** are also demonstrated by the column sorption experiments discussed as follows.

(vii) Column sorption studies. As industrial water treatment requires the use of ion-exchange columns, we have investigated the capability of **BUT-MOF** to absorb toxic anions under continuous flow conditions. As in our previous column sorption studies with other Zr^{4+} MOFs,[15,16] **BUT-MOF** was used in its composite form with alginic acid (HA) and the column fabricated contained a mixture of silica sand (99 wt%) and **BUT-MOF/HA** (1 wt%) as the stationary phase. Taking into account the results from batch sorption studies revealing extraordinary selectivity of **BUT-MOF** towards Se(IV), we have chosen Se(IV) as the target anion to be removed from water samples containing 1 ppm of Se (total Se content). After passing 140 mL of the Se(IV)-containing solution, through the column, the determined Se content was <10 ppb, *i.e.* below the acceptable Se concentration in water (Fig. S25†). The column was regenerated by treating it with 4 M HCl and reused for Se(IV) sorption. In the second run, again 140 mL of the solution can be decontaminated (*i.e.* contained <10 ppb of Se) after passing it through the column (Fig. S25†). A third run, after regeneration of the column, gave similar results as those in the previous runs (Fig. S25†). The above data revealed that **BUT-MOF** is promising for sorption applications under continuous flow conditions.

(viii) Comparison of BUT-MOF and analogues with other anion MOF sorbents. Tables S9 and S10† summarize the most important sorption properties of various MOFs and other types of sorbents, for Se(IV/VI) removal.[17,18,28–35] **BUT-MOF** and other analogues shows the highest Se(IV) and Se(VI) sorption capacities among other MOFs (Table S9†). Remarkably, the Se(VI) sorption capacities of the alkylamino-functionalized MOFs are (at least) two times larger than those of best known MOF sorbents.[17,18,28–32] **BUT-MOF** and other analogues show higher or comparable Se(IV/V) sorption capacities with those of other types of sorbents (besides MOFs), with the exception of a thiourea-formaldehyde (TUF) resin which displays significantly higher Se(IV/VI) sorption capacities than those of the alkyl-amino functionalized Zr^{4+} MOFs (Table S10†).[33–35] Nevertheless, TUF resin is effective for Se(IV/VI) sorption only at very acidic conditions (pH < 1) showing also very slow sorption kinetics (equilibrium time = 78 h). In addition, the selectivity and reusability of this sorbent are unclear. In contrast, **BUT-MOF** is efficient for Se(IV/VI) sorption over a wider pH range (1–10) compared to the

operating pH range of other sorbents. In addition, the Se(IV/VI) sorption kinetics of the MOFs reported here (equilibrium time 1–3 min) compares well with that of NU-1000 showing the fastest Se(IV/VI) sorption among MOFs.[17,18] We should also note that the alkylamino-functionalized Zr^{4+} MOFs presented here show an exceptional selectivity for selenite, which is reminiscent that of a Bi^{3+} MOF reported recently.[29] However, the latter cannot be regenerated and reused, whereas the new Zr^{4+} MOFs retain their initial selenite sorption capacity after several (at least three) cycles of regeneration–reuse. Importantly, the reported **BUT-MOF** and the other alkylamino-functionalized analogues are the only MOFs reported so far that are capable to remove $SeCN^-$. Till now, a few ion-exchange resins have been studied for $SeCN^-$ sorption revealing much lower $SeCN^-$ sorption capacities (126 and 178 mg g^{-1} for Smopex®-269 and Smopex®-103, respectively) compared to those of MOFs reported in this work.[27]

(d) Mechanism of ion sorption

(i) General remarks. As mentioned above, **BUT-MOF** was activated with 4 M HCl solution and then washed with water to remove the excess of HCl. EDS analysis of the acid-treated MOF revealed only a small amount of Cl (Zr : Cl atomic ratio was ~6 : 1). This Cl content was similar in the anion-loaded materials, thus indicating that Cl is not exchangeable and may be in the form of HCl strongly bound to the surface of particles. Therefore, it is apparent that the capability of **BUT-MOF** and its analogues to absorb anionic Se species is not due to exchange process involving extra-framework anions. Nevertheless, the protonation of the MOF enhances the sorption kinetics as the deprotonated MOF (MOF pre-treated with a base) requires ~4 h to achieve the sorption equilibrium (whereas the equilibrium is achieved within 1–3 min by the protonated MOF). This finding reveals that the sorption process involves in some degree binding of anions into the charged surface of the MOF particles. Indeed, zeta potential measurements indicated a value of +24.2 ± 5.0 mV revealing the positive surface charge of MOF particles. However, the exceptional capture of Se-anions by the MOFs could not be explained only on the basis of surface sorption. According to previous works describing anion sorption by 8-c Zr^{4+} MOFs,[15–19] the terminal OH/H_2O terminal ligands of the Zr_6 clusters constitute the sorption sites in which the anions are grafted. Specifically, the insertion of various anions is accompanied by release of terminal OH^- ligands and thus, the sorption process proceeds *via* an anion exchange mechanism. Therefore, such intra-framework anion sorption can also contribute to the highly efficient capture of Se anionic species by the MOFs, besides the contribution of surface binding.

(ii) Solid state characterization of the ion-loaded MOFs. The characterization of ion-loaded **BUT-MOF** materials has been performed with various methods including IR, BET surface area determination and PXRD. IR data indicate characteristic bands of the inserted anions (Fig. S26†). The ion-loaded materials display decreased BET surface areas (402–544 m^2 g^{-1}, Fig. S27†) compared to that of pristine MOF. This indicates that the sorption of anions occurs not only in the surface, but also insides the pores of **BUT-MOF**. The structure of **BUT-MOF** is retained after the anion-sorption processes, as revealed by comparison of the PXRD patterns and subsequently indexing and structureless refinement (Fig. S28–S30†). The anion-loaded materials exhibited sufficiently high crystallinity and thus, we were able to solve and refined the structures of these materials *via* PXRD methods. According to sorption data, ~2 equivalents of SeO_4^{2-} anions are sorbed per **BUT-MOF** formula. Specifically, the intra-framework sorption of SeO_4^{2-} by **BUT-MOF** may proceed *via* replacement of terminal hydroxyl ligands from the Zr_6 clusters and binding of the inserted anionic species to the Zr^{4+} centers, as shown in the following equation:

$$H_{16}[Zr_6O_{16}(BUTNH\text{-}BDC)_4] + 2SeO_4^{2-} \rightarrow H_{12}[Zr_6O_{12}(SeO_4)_2(BUTNH\text{-}BDC)_4] + 4OH^- \quad (1)$$

Thus, we built a model in which 2 SeO_4^{2-} anions replace four terminal ligands on the equatorial plane of the Zr_6 core and connect to the Zr^{4+} metal ions in a n^1, n^1:μ_2-fashion (such coordination mode is commonly observed in Se(IV/VI)-loaded Zr^{4+} MOFs).[17,18,32] We have also included water molecules in the pores of **BUT-MOF/SeO_4^{2-}** material. After the successful optimization of this model, Rietveld refinement was carried out to obtain the final structure (Fig. 8A). The results of the refinement were very satisfying (Fig. S28†) indicating the correctness of the proposed structural model.

As mentioned above, Se(IV) exists as $HSeO_3^-$ and SeO_3^{2-} at neutral and alkaline (pH > 9) solutions respectively. Thus, the predicted sorption capacities of **BUT-MOF** would be 4 and 2 moles of Se(VI) per formula unit of **BUT-MOF** at pH ~ 7 and pH > 9 respectively:

$$H_{16}[Zr_6O_{16}(BUTNH\text{-}BDC)_4] + 4HSeO_3^- \rightarrow H_4[Zr_6O_8(HSeO_3)_4(BUTNH\text{-}BDC)_4] + 4OH^- + 4H_2O \ (pH \sim 7) \quad (2)$$

$$H_{16}[Zr_6O_{16}(BUTNH\text{-}BDC)_4] + 2SeO_3^{2-} \rightarrow H_{12}[Zr_6O_{12}(SeO_3)_2(BUTNH\text{-}BDC)_4] + 4OH^- \ (pH > 9) \quad (3)$$

We have found somewhat higher $HSeO_3^-$ sorption capacity (5.0 mol mol^{-1} or 272 mg g^{-1} of **BUT-MOF**) than the predicted one (4.0 mol mol^{-1} or 217 mg g^{-1} of **BUT-MOF**). It is likely that 4 $HSeO_3^-$ replaced the terminal OH/H_2O ligands from the Zr_6 clusters and the remaining $HSeO_3^-$ (1 mol mol^{-1} or 55 mg g^{-1} of **BUT-MOF**) was captured at the external surface of particles through $-NH_2^+(R)\cdots HSeO_3^-$ electrostatic interactions (and hydrogen bonds between $HSeO_3^-$ and carbonyl oxygen atoms, see below). The external surface sorption of $HSeO_3^-$ is relatively limited (being only 20% of the total $HSeO_3^-$ sorption capacity of **BUT-MOF**) and as a result, it is not appeared as a separate step in the $HSeO_3^-$ sorption isotherm (Fig. 6). For comparison, the external surface sorption of Se(VI) or $SeCN^-$ species by **BUT-MOF** reaches up to 50% of the total sorption capacities, thus resulting in sorption isotherms with two components (Fig. 6).

In contrast, the experimental SeO_3^{2-} sorption capacity (2.2 mol mol^{-1} **BUT-MOF**, pH ~ 9.5) was nearly equal to the calculated. At alkaline conditions, amine groups are

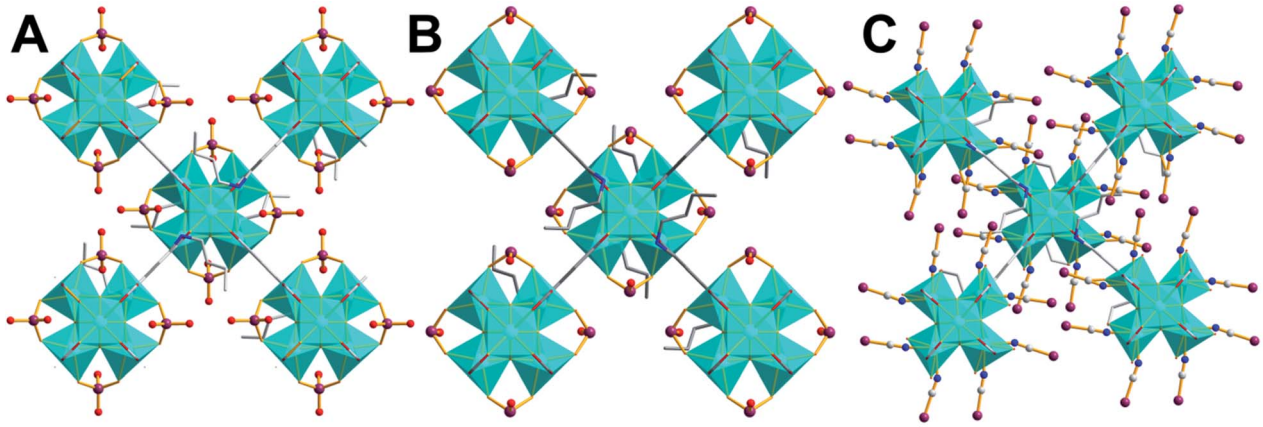

Fig. 8 Structures of (A) **BUT-MOF/SeO_4^{2-}**, (B) **BUT-MOF/$HSeO_3^-$** and (C) **BUT-MOF/$SeCN^-$**. For clarity, to eliminate positional disorder of butyl and Se-groups, the structures are shown as the low symmetry *I*4̄ models. H atoms were omitted. Color code: Zr, cyan; N, blue; O, red; C, grey; Se, plum.

deprotonated and thus, surface sorption is less favoured. As a result, the sorption of Se(IV) anions occurs mainly into the Zr_6 clusters of the framework.

Based on the above, the structural model we built for the **BUT-MOF/$HSeO_3^-$** included 4 Se(IV) species coordinated in n^1, n^1:μ_2-fashion to the Zr^{4+} metal centers as well as water molecules in the pores (Fig. 8B). The model was optimized and used as starting point for Rietveld refinement, which gave satisfactory results (Fig. S29†).

Based on isotherm sorption studies, **BUT-MOF** captures $SeCN^-$ *via* a two-step process: (i) surface sorption (lower concentration range) and (ii) intra-framework sorption (higher concentration range). The intra-framework $SeCN^-$ sorption can be described by the following equation:

$$H_{16}[Zr_6O_{16}(BUTNH\text{-}BDC)_4] + 4SeCN^- \rightarrow H_{12}[Zr_6O_{12}(SeCN)_4(BUTNH\text{-}BDC)_4] + 4OH^- \quad (4)$$

We thus built and optimize a model in which four $SeCN^-$ coordinate to the Zr^{4+} metal ions in a monodentate fashion (Se–CN···Zr) replacing half of the terminal water/OH^- ligands (Fig. 8C). Such coordination mode is also supported by IR data (Fig. S26†). This structural model was used as starting point for Rietveld refinement, which provided fairly good results (Fig. S30†).

(iii) Explanation of the higher affinity of MOFs for Se(IV). From the above studies, it became clear that the selenite sorption by the MOFs is not affected by excess of several competitive anionic species (*e.g.* SO_4^{2-}, HCO_3^-), whereas the capture of the other Se species is somewhat inhibited in the presence of high concentrations of competitive anions (especially in the presence of HCO_3^-).

According to the sorption data described above, the anions can bind to the positively charged surface of the particles, *i.e.* to the protonated amine groups of the surface ligands, as well as ligate with the Zr^{4+} metal ions. In order to explain the higher selectivity of the MOFs towards $HSeO_3^-$, we should consider both ligation capability of the various anionic species and their interactions with the functional groups of the ligands. To this end, we have performed theoretical calculations.

Fig. S31† shows the natural atomic charges of SeO_4^{2-}, $HSeO_3^-$, $SeCN^-$, SO_4^{2-} and HCO_3^- calculated by the natural bond orbital (NBO) population analysis using Weinhold's methodology.[36,37] Based on the charge values of donor atoms (O or N) of the anionic species, we may have an estimation of the ligation efficiency of the anions towards the hard Zr^{4+} metal ions. Thus, SeO_4^{2-}, $HSeO_3^-$ and SO_4^{2-} including O atoms with quite close charge values (−1.044 to −1.161) are expected to display similar ligation capability for Zr^{4+} and higher than that of HCO_3^- containing O atoms with lower charge values (−0.822 to −0.844). In addition, the negative charge of N atom (−0.581) of $SeCN^-$ is significant smaller than that of O atoms of the other anionic species and thus, $SeCN^-$ is anticipated to be less effective ligand for Zr^{4+} compared to other anions. Therefore, the higher affinity of the MOFs for $HSeO_3^-$ cannot be explained only on the basis of its capability for ligation with Zr^{4+}.

To get insight into the interactions of the various anions with the ligands of the MOF materials, we calculated the interaction energies of $HSeO_3^-$, SeO_4^{2-}, $SeCN^-$, SO_4^{2-} and HCO_3^- anions with *N*-alkyl-2,5-bis(methoxycarbonyl)benzenaminium, as a model for the MOF's ligand, at the B3LYP/6-31+G(d)/PCM level of theory in aqueous solution using the Gaussian 09, version D.01 program suite.[38] The optimized geometries of the possible MOF@$SeCN^-$, MOF@$HSeO_3^-$, MOF@SeO_4^{2-}, MOF@SO_4^{2-} and MOF@HCO_3^- weak associations supported by hydrogen bonds and Coulomb (electrostatic) forces, along with selected structural parameters and the interaction energies (ΔE in kcal mol^{-1}) and enthalpy changes (ΔH in kcal mol^{-1}) calculated at the B3LYP/6-31+G(d)/PCM level of theory in aqueous solution, are shown in Fig. S32.†

It can be seen that the SeO_4^{2-} dianions are the most strongly associated species with the MOF's ligand, followed by the SO_4^{2-} dianions and the $SeCN^-$ anionic species. Notice that the interactions are primarily electrostatic in nature in synergy with hydrogen bond formation. The $HSeO_3^-$ and HCO_3^- anions can be associated with the ligand by three different interaction

modes (Fig. S32†), since the OH group of these species can participate in hydrogen bond formation with the carbonyl oxygen atoms of the ligand. The estimated interactions energies for the three interaction modes of the $HSeO_3^-$ and HCO_3^- species with the MOF's ligand are smaller than the corresponding interactions energies of the selenate, sulfate and selenocyanate anions. However, the possibility of the $HSeO_3^-$ and HCO_3^- anions to interact with the ligand in three different interaction modes allows more ($HSeO_3^-$ or HCO_3^-) species to be associated to the MOF's moiety than the $SeCN^-$, SeO_4^{2-} and SO_4^{2-} species, which likely explains (a) the higher selectivity of the MOFs for $HSeO_3^-$ *vs.* $SeCN^-$, SeO_4^{2-} and SO_4^{2-} and (b) the negligible $SeCN^-$, SeO_4^{2-} sorption capacity of the MOFs in the presence of excess of HCO_3^-. Finally, the fact that $HSeO_3^-$ may be more efficient ligand for Zr^{4+} than HCO_3^- (see above) accounts for the observed selectivity of the MOFs for $HSeO_3^-$ in the presence of excess of HCO_3^-.

Conclusions

In the present work, we demonstrated that the utilization of terephthalic linkers with slightly to moderately elongated functional groups, such as RNH- (R = ethyl, propyl, isobutyl, *n*-butyl), constitutes an effective synthetic strategy towards the isolation of Zr^{4+} MOF with decreased net (8-c) connectivity. The new MOFs with relatively small-sized functional groups showed substantially higher surface areas (up to 832 $m^2\ g^{-1}$) than that (354 $m^2\ g^{-1}$) of **MOR-2** (the only other known Zr^{4+}-MOF with a terephthalate linker and 8-c framework) incorporating bulky (2-picolylamino) functionalities. Presumably, even small-sized groups, such as ethyl-, propyl-amino *etc.*, cause significant steric interactions between the linkers resulting to the stabilization of the observed 8-connected rather than the usual 12-connected frameworks. The targeted synthesis of Zr^{4+} MOFs with low-net connectivity is highly desirable, not only as a means for the isolation of materials with enhanced porosity, but also as an approach to introduce intra-framework anion sorption sites (*i.e.* labile terminal water/hydroxy ligands). Actually, the sorption capacities of the reported MOFs for the toxic Se(IV/VI)-based anions surpass that of known MOFs and most of other materials. Remarkably, the Se(VI) sorption capacities of the MOFs are more than double compared to other MOF sorbents and the Se(IV) sorption by the reported alkylamino-functionalized MOFs is extraordinary (removal capacities >98% in ≤3 min) even in the presence of a tremendous (>200-fold) excess of various competitive anions. The highly efficient Se(IV) and Se(VI) capture by the MOFs is due to a dual sorption process involving both surface binding (*via* electrostatic-hydrogen bonding interactions) and intra-framework sorption *via* replacement of the terminal H_2O/OH^- ligands by the inserted Se anions. In addition, the new MOFs showed an exceptional capability to sorb $SeCN^-$ species, a particularly toxic Se form, with such sorption property presented for the first time for MOF materials. Again, the $SeCN^-$ capture involves both surface and intra-framework sorption. Importantly, the $SeCN^-$ sorption capacities of the new MOFs are superior to those of other sorbents tested so far. Additional toxic anionic species may be efficiently sorbed by the alkylamino-functionalized MOFs. Such investigations are underway.

Author contributions

A. D. Pournara: investigation, formal analysis, writing-original draft, S. Rapti: investigation, formal analysis, A. Valmas: investigation, writing-original draft, I. Margiolaki: investigation, resources, E. Andreou: investigation, formal analysis, G. S. Armatas: investigation, formal analysis, writing-review & editing, resources, A. C. Tsipis: investigation, formal analysis, resources, writing-original draft, J. C. Plakatouras: investigation, formal analysis, writing-review & editing, D. L. Giokas: investigation, formal analysis, resources, writing-review & editing, M. J. Manos: conceptualization, supervision, resources, writing-original draft.

Conflicts of interest

There are no conflicts to declare.

Acknowledgements

The research work was supported by the Hellenic Foundation for Research and Innovation (H.F.R.I.) under the "First Call for H.F.R.I. Research Projects to support Faculty members and Researchers and the procurement of high-cost research equipment grant" (Project Number: 348).

Notes and references

1 M. Eddaoudi, D. B. Moler, H. Li, B. Chen, T. M. Reineke, M. O'Keeffe and O. M. Yaghi, *Acc. Chem. Res.*, 2001, **34**, 319–330.
2 G. Férey, *Chem. Soc. Rev.*, 2008, **37**, 191–214.
3 S. Horike, S. Shimomura and S. Kitagawa, *Nat. Chem.*, 2009, **1**, 695–704.
4 D. Bradshaw, J. B. Claridge, E. J. Cussen, T. J. Prior and M. J. Rosseinsky, *Acc. Chem. Res.*, 2005, **38**, 273–282.
5 O. K. Farha and J. T. Hupp, *Acc. Chem. Res.*, 2010, **43**, 1166–1175.
6 S. Zheng, T. Wu, J. Zhang, M. Chow, R. A. Nieto, P. Feng and X. Bu, *Angew. Chem., Int. Ed.*, 2010, **49**, 5362–5366.
7 D. Sheng, L. Zhu, X. Dai, C. Xu, P. Li, C. I. Pearce, C. Xiao, J. Chen, R. Zhou, T. Duan, O. K. Farha, Z. Chai and S. Wang, *Angew. Chem., Int. Ed.*, 2019, **58**, 4968–4972.
8 C. Xiao, A. Khayambashi and S. Wang, *Chem. Mater.*, 2019, **31**, 3863–3877.
9 P. Kumar, A. Pournara, K. H. Kim, V. Bansal, S. Rapti and M. J. Manos, *Prog. Mater. Sci.*, 2017, **86**, 25–74.
10 J. Li, X. Wang, G. Zhao, C. Chen, Z. Chai, A. Alsaedi, T. Hayat and X. Wang, *Chem. Soc. Rev.*, 2018, **47**, 2322–2356.
11 A. V. Desai, S. Sharma and S. K. Ghosh, in *Metal-Organic Frameworks (MOFs) for Environmental Applications*, Elsevier, Amsterdam, 2019, pp. 95–140.

12 Z. L. Magnuson and S. Ma, in *Metal-Organic Frameworks (MOFs) for Environmental Applications*, Elsevier, Amsterdam, 2019, pp. 63–93.
13 Y. Bai, Y. Dou, L. H. Xie, W. Rutledge, J. R. Li and H. C. Zhou, *Chem. Soc. Rev.*, 2016, **45**, 2327–2367.
14 Z. Hu and D. Zhao, *Dalton Trans.*, 2015, **44**, 19018–19040.
15 S. Rapti, D. Sarma, S. A. Diamantis, E. Skliri, G. S. Armatas, A. C. Tsipis, Y. S. Hassan, M. Alkordi, C. D. Malliakas, M. G. Kanatzidis, T. Lazarides, J. C. Plakatouras and M. J. Manos, *J. Mater. Chem. A*, 2017, **5**, 14707–14719.
16 S. Rapti, S. A. Diamantis, A. Dafnomili, A. Pournara, E. Skliri, G. S. Armatas, A. C. Tsipis, I. Spanopoulos, C. D. Malliakas, M. G. Kanatzidis, J. C. Plakatouras, F. Noli, T. Lazarides and M. J. Manos, *J. Mater. Chem. A*, 2018, **6**, 20813–20821.
17 A. J. Howarth, M. J. Katz, T. C. Wang, A. E. Platero-Prats, K. W. Chapman, J. T. Hupp and O. K. Farha, *J. Am. Chem. Soc.*, 2015, **137**, 7488–7494.
18 A. J. Howarth, Y. Liu, J. T. Hupp and O. K. Farha, *CrystEngComm*, 2015, **17**, 7245–7253.
19 R. J. Drout, K. Otake, A. J. Howarth, T. Islamoglu, L. Zhu, C. Xiao, S. Wang and O. K. Farha, *Chem. Mater.*, 2018, **30**, 1277–1284.
20 E. D. Van Hullebusch, *Bioremediation of Selenium Contaminated Wastewater*, Springer, Switzerland, 2017, pp. 1–130.
21 L. Sarkisov and A. Harrison, *Mol. Simul.*, 2011, **37**, 1248–1257.
22 The calculations of the surface areas and pore sizes using poreblazer were done using a lower symmetry model ($I\bar{4}$) of the structures, without guests in the pores. In these models, there are no positional disordered groups. In the structural models with the *I*4/*m* space group, there are duplicates of atoms due to their positional disorder. Thus, the structures appear erroneously denser and the calculations lead to incorrect results.
23 J. Torres, V. Pintos, S. Domínguez, C. Kremer and E. Kremer, *J. Solution Chem.*, 2010, **39**, 1–10.
24 J. Kretzschmar, N. Jordan, E. Brendler, S. Tsushima, C. Franzen, H. Foerstendorf, M. Stockmann, K. Heim and V. Brendler, *Dalton Trans.*, 2015, **44**, 10508–10515.
25 Y. Georgiou, S. Rapti, A. Mavrogiorgou, G. Armatas, M. J. Manos, M. Louloudi and Y. Deligiannakis, *Sci. Rep.*, 2020, **10**, 1–12.
26 S. Soda, M. Kashiwa, T. Kagami, M. Kuroda, M. Yamashita and M. Ike, *Desalination*, 2011, **279**, 433–438.
27 C. Mac Namara, J. Torroba and A. Deacon, *Johnson Matthey Technol. Rev.*, 2015, **59**, 334–352.
28 J. Wei, W. Zhang, W. Pan, C. Li and W. Sun, *Environ. Sci.: Nano*, 2018, **5**, 1441–1453.
29 H. Ouyang, N. Chen, G. Chang, X. Zhao, Y. Sun, S. Chen, H. Zhang and D. Yang, *Angew. Chem., Int. Ed.*, 2018, **57**, 13197–13201.
30 J. Li, Y. Liu, X. Wang, G. Zhao, Y. Ai, B. Han, T. Wen, T. Hayat, A. Alsaedi and X. Wang, *Chem. Eng. J.*, 2017, **330**, 1012–1021.
31 S. Sharma, A. V. Desai, B. Joarder and S. K. Ghosh, *Angew. Chem., Int. Ed.*, 2020, **59**, 7788–7792.
32 R. J. Drout, A. J. Howarth, K. I. Otake, T. Islamoglu and O. K. Farha, *CrystEngComm*, 2018, **20**, 6140–6145.
33 L. Ma, S. M. Islam, C. Xiao, J. Zhao, H. Liu, M. Yuan, G. Sun, H. Li, S. Ma and M. G. Kanatzidis, *J. Am. Chem. Soc.*, 2017, **139**, 12745–12757.
34 N. Gezer, M. Gülfen and A. O. Aydín, *J. Appl. Polym. Sci.*, 2011, **122**, 1134–1141.
35 L. Zhu, L. Zhang, J. Li, D. Zhang, L. Chen, D. Sheng, S. Yang, C. Xiao, J. Wang, Z. Chai, T. E. Albrecht-Schmitt and S. Wang, *Environ. Sci. Technol.*, 2017, **51**, 8606–8615.
36 A. E. Reed, L. A. Curtiss and F. Weinhold, *Chem. Rev.*, 1988, **88**, 899–926.
37 F. Weinhold, in *Encyclopedia of Computational Chemistry*, Wiley, Chichester, UK, 1998, pp. 1792–1811.
38 M. J. Frisch, G. W. Trucks, H. B. Schlegel, G. E. Scuseria, M. A. Robb, J. R. Cheeseman, G. Scalmani, V. Barone, B. Mennucci, G. A. Petersson, H. Nakatsuji, M. Caricato, X. Li, H. P. Hratchian, A. F. Izmaylov, J. Bloino, G. Zheng, J. L. Sonnenberg, M. Hada, M. Ehara, K. Toyota, R. Fukuda, J. Hasegawa, M. Ishida, T. Nakajima, Y. Honda, O. Kitao, H. Nakai, T. Vreven, J. A. Montgomery Jr, J. E. Peralta, F. Ogliaro, M. Bearpark, J. J. Heyd, E. Brothers, K. N. Kudin, V. N. Staroverov, R. Kobayashi, J. Normand, K. Raghavachari, A. Rendell, J. C. Burant, S. S. Iyengar, J. Tomasi, M. Cossi, N. Rega, M. J. Millam, M. Klene, J. E. Knox, J. B. Cross, V. Bakken, C. Adamo, J. Jaramillo, R. Gomperts, R. E. Stratmann, O. Yazyev, A. J. Austin, R. Cammi, C. Pomelli, J. W. Ochterski, R. L. Martin, K. Morokuma, V. G. Zakrzewski, G. A. Voth, P. Salvador, J. J. Dannenberg, S. Dapprich, A. D. Daniels, Ö. Farkas; J. B. Foresman, J. V. Ortiz, J. Cioslowski and D. J. Fox, *Gaussian 09, Revision D.01*, Gaussian, Inc., Wallingford, CT, 2010.